Article

Journal of the Brazilian Chemical Society

https://dx.doi.org/10.21577/0103-5053.20240197

J. Braz. Chem. Soc. **2025**, *36*, 5, e-20240197, 1-12

Dye Contaminant Removal: Adsorption on Thermoplastic Starch/Kraft Lignin Composites and Photodegradation

Amanda S. M. de Freitas,[a] *Jéssica S. Rodrigues,*[b] *Stefanny F. Amaro,*[a] *Beatriz M. Ramos*[a] *and Marystela Ferreira*[*,a]

[a]*Centro de Ciência e Tecnologia para a Sustentabilidade (CCTS), Universidade Federal de São Carlos (UFSCar), 18052-780 Sorocaba-SP, Brazil*

[b]*Instituto de Ciência e Tecnologia (ICT), Universidade Estadual Paulista (Unesp), 18087-180 Sorocaba-SP, Brazil*

This study investigated the removal of contaminants in water by adsorption on thermoplastic starch (TPS) and kraft lignin (KL) composites. A study on the desorption of methylene blue (MB) and methyl orange (MO) dyes in water was also carried out, followed by the photodegradation of solutions containing dissolved dyes. Initially, the surface morphology of the TPS and TPS-KL films was analyzed by scanning electron microscopy, revealing advantageous characteristics for efficient adsorption of contaminants. Fourier transform infrared spectroscopy (FTIR) analysis made it possible to characterize the TPS and TPS-KL composites. The results demonstrate the reversibility of the process and confirm the lack of permanent chemical modification in the polymer matrix, indicating that the adsorption/desorption process is physical rather than chemical. This suggests that the adsorbent material can be reused without losing its fundamental structural properties. Furthermore, the study allows for verification of the chemical changes on the surfaces of the materials involved. Ultraviolet-visible spectroscopy (UV-Vis) results show that for MO, both substrates exhibited low adsorption capacity, with efficiency values close to 20%. In contrast, for MB, both composite materials displayed excellent dye adsorption rates, achieving efficiencies of 78% or higher. The photodegradation of adsorbed dyes revealed promising results.

Keywords: adsorption, desorption, photodegradation, water remediation, dyes

Introduction

For years, water resources have been altered by human activities and this occurs due to the demand for water use by humans, which results in damaging environmental issues such as the pollution of rivers, seas, and lakes, reducing the quality and availability of water, which in turn, result in more consequences for the environment.[1] Significantly, the effluents containing reactive dyes discharged by textile industries are responsible for approximately 17 to 20% of global water pollution. Dyes are predominantly employed to add color to textiles and various other materials.[2]

The effluent from textile production often contains a range of harmful dye molecules, presenting a serious environmental hazard. Methylene blue (MB), a commonly used cationic dye from the thiazine family known for its stability in water at room temperature, is consistently detected in textile wastewater. Methyl orange (MO) dye is also an effluent from the textile industry; however, it is anionic.[3] Dye molecules, along with other dyes present in textile effluents, present challenges for treatment processes due to their resistance to biodegradation. However, the adsorption method has emerged as a promising approach for MB and MO removal, offering rapid kinetics, simple design and operation, and low cost.[4]

Adsorption consists of the adhesion of molecules of a fluid (the adsorbate) to a solid surface (the adsorbent). Adhesion can be physical (physisorption), characterized by Van der Waals interactions, or chemical (chemisorption), through which the active sites of the adsorbent are connected through chemicals bonds with the compounds. Since this mass concentration of the adsorbate occurs on the external surface of solids, the larger this surface is *per* unit of solid mass, the more favorable the adsorption will be.[5] This means that the materials on which the interest substance

*e-mail: marystela@ufscar.br
Editor handled this article: Fernando C. Giacomelli (Associate)

will be adsorbed are generally porous solids. While the phenomenon of adsorption occurs, a desorption process occurs, where some adsorbate molecules detach from the solid surface of the adsorbent and return to the solution. As soon as the speeds of adsorption and desorption become equal and thereafter remain constant, it is concluded that the system has reached equilibrium.[6]

In this context, contamination of water by dyes can be minimized using the adsorption of dye molecules by a polymeric matrix. To minimize environmental impacts, one of the polymers with great potential for the development of biodegradable materials is starch, whose structure is formed by glucose monomers,[7] being able to be metabolized by microorganisms, and kraft lignin, a promising ultraviolet (UV) protection material to replace synthetic absorbents in a composite due to its excellent property of protection against UV rays, assisting in processes of photodegradation.[8]

This work proposes the preparation of substrates with sustainable, low-cost, and biodegradable materials that have a high capacity for desorbing dyes, which could make reuse feasible. In addition to making comparisons between the adsorption capacity of pure thermoplastic starch (TPS) and that added with kraft lignin, which is an industrial by-product. The study of two dyes, one anionic and the other cationic, in terms of their ability to adsorb, desorb and decontaminate dyes desorbed by the photodegradation process, which does not generate chemical waste, broadens the scope of the research. This study investigated the removal of contaminants from water by adsorption onto thermoplastic starch (TPS) and kraft lignin (KL) composites. A study was carried out on the desorption of methylene blue (MB) and methyl orange (MO) dyes in water, followed by the photodegradation of solutions containing dissolved dyes.

Experimental

Reagents and solution

The starch used was AMIDEX 3001, supplied by DAXIA (São Paulo, Brazil) (characteristics: maximum moisture content 14%; pH 4.5-5.5). The lignin utilized was extracted from *Eucalyptus urograndis* through the kraft process, employed in the production of cellulose and paper, and was supplied by Suzano, located in São Paulo, Brazil. Other reagents included glycerin P.A. (glycerol), supplied by Anidrol Laboratory Products (Diadema, Brazil); dimethylsulfoxide P.A. (DMSO), supplied by Labsynth (São Paulo, Brazil); methyl orange (MO), supplied by LAC - Laboratory Products (Araraquara, Brazil); and methylene blue (MB), supplied by Sigma-Aldrich (Missouri, USA). All solutions used in this study were prepared using ultrapure water (Sartorius Weighing Technology, Göttingen, Germany), with a resistivity of 18.2 MΩ cm at 25 °C.

Film preparation

Thermoplastic starch

A solution containing 110 g of ultrapure water, 30 g of starch, and 10 g of glycerol was heated with stirring until it reached approximately 80 °C and maintained at this temperature for 5 min. The resulting solution was then aliquoted into Falcon tubes, filling approximately one-third of their total volume capacity (around 15 mL), capped, and placed in a freezer at –18 °C for 24 h. Subsequently, the frozen samples were transferred to a freeze-dryer, model Enterprise I, brand Terroni (São Carlos, Brazil) for 24 h under a vacuum of 260 μHg and at a temperature of 0 °C. Upon removal from the freeze-dryer, the samples were ground using an IKA®, model A11 basic analysis mill (Campinas, Brazil).

TPS and TPS-KL films

The films were fabricated using the casting technique,[9] which involves dehydrating the film-forming solution applied to Petri dishes. For the TPS, a mixture of thermoplastic starch (prepared beforehand with granular starch and glycerin as a plasticizer) and dimethyl sulfoxide (DMSO) served as the base. In the case of TPS-KL films, 4% lignin (m/m) was incorporated alongside DMSO.

The films were prepared following the methodology described by Freitas *et al*.[8] Film-forming solutions were continuously stirred and heated to approximately 80 °C for about 10 min to ensure material gelatinization. Subsequently, approximately 25 g of film material was molded into Petri dishes and dried in an oven at 40 °C for 48 h, followed by 80 °C for 8 h. Each film was replicated three times. After drying, the material underwent a pressure of 2.0 tons for 5 min to compact the substrate and was then cut into small rectangles.

Characterization techniques

Fourier-transform infrared spectroscopy (FTIR)

The structural characterization of the films was conducted using the Nicolet Summit, IR 200 FTIR model, by Thermo Fisher Scientific Inc. (Massachusetts, USA) in attenuated total reflectance (ATR) mode at room temperature, with 126.0 scans and a nominal resolution of 4.0 cm^{-1}, covering the spectrum range from 4000 to 400 cm^{-1}.

The spectra were obtained with Paradigma Ominic (Thermo Scientific, USA) and through Origin Pro 8.5.[10]

Scanning electron microscopy (SEM)

SEM analysis was conducted using a TM 3000 microscope, by Hitachi (Tokyo, Japan), operating under variable pressure vacuum conditions, with an acceleration voltage of 15 kV and surface magnifications of 50 and 80×. The instrument was equipped with a backscattered electron detector. The micrographs obtained were collected and treated using the Microsoft Power Point[11] program. Initially, the surfaces of the films were examined, followed by analysis after dye adsorption, and finally after dye desorption.

Ultraviolet-visible spectroscopy (UV-Vis)

Monitoring adsorption/desorption by UV-Vis

The UV-Vis spectrophotometer used in this study was a Genesys model, by Thermo Fisher Scientific Inc. (Massachusetts, USA). The data obtained were collected and processed using Origin 8.5 software.[10] Its purpose was to investigate how contact time affected dye adsorption by the produced films. A quartz cell with an optical path length of 1.0 cm was used to establish the dye concentration calibration curve. This cuvette contained aliquots of methyl orange solution at concentrations ranging from 2 to 10 mg L^{-1}. The adsorption spectra were subsequently recorded within the wavelength range of 400 to 700 nm. The coloration of dyes is usually attributed to the presence of chromophore groups, unsaturation, present in the chemical structure of the compounds which is shown in Figure 1.

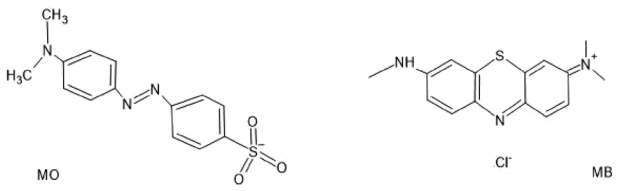

Figure 1. Chemical structure of the dyes methyl orange (MO) and methylene blue (MB).

The adsorption wavelength for MO was determined to be 465 nm according to a previous study.[12] A similar procedure was applied for MB, with a spectral range of 450 to 700 nm. The maximum absorption for MB was observed at 600 nm.[13] Adsorption experiments involved immersing the TPS and TPS-KL films in an aqueous solution containing MB at a concentration of 10 mg L^{-1} for 8 h (Figure 2a). UV-Vis measurements of the solution were taken hourly. A similar procedure was followed for an aqueous solution of MO at a concentration of 10 mg L^{-1}.

All experiments were conducted in triplicate to facilitate data processing, enabling the calculation of mean values and standard deviations.

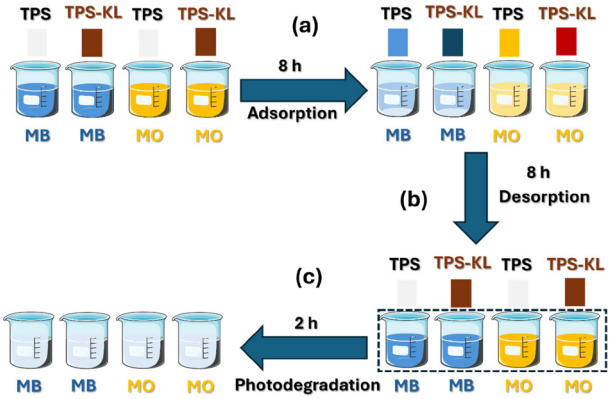

Figure 2. Experimental: (a) adsorption of the dyes (methylene blue (MB) and methyl orange (MO)) from solution onto films (thermoplastic starch (TPS) and TPS/kraft lignin (TPS-KL)); (b) desorption of these dyes from the films; (c) photodegradation of the desorbed dyes in water.

Adsorption kinetics

Adsorption kinetic models were proposed based on the results obtained by UV-Vis for the adsorption of dyes on TPS and TPS-KL substrates. The pseudo-first and pseudo-second-order models allow us to assess whether the observed adsorption kinetics fit a kinetic model. The pseudo-first-order model was first proposed by Lagergren,[14] in 1898, and is represented by equation 1.

$$\frac{dqt}{dt} = K_1(q_e - q_t) \quad (1)$$

where K_1 is the pseudo-first-order adsorption rate constant (s^{-1}); q_e is the amount of analyte adsorbed at equilibrium (mg g^{-1}); q_t is the amount of analyte adsorbed in each time interval (mg g^{-1}); t is the adsorption time (s).

The pseudo-second-order kinetic model is given by equation 2.

$$\frac{dqt}{dt} = K_2(q_e - q_t)^2 \quad (2)$$

where K_2 is the pseudo-second-order adsorption rate constant (g mg^{-1} s^{-1}); q_e is the amount of analyte adsorbed at equilibrium (mg g^{-1}); q_t is the amount of analyte adsorbed in each time interval (mg g^{-1}); t is the adsorption time (s). The minimum value of the correlation coefficient (R^2) and the adsorption rate values (K_2) were also presented. The R^2 values obtained for each model (pseudo-first and second order) were used to evaluate the fit to the kinetic model with the most favorable order.

Desorbed dye and photodegradation test

To initiate the desorption process, the films with adsorbed dyes were immersed in milli-Q water. UV-Vis measurements of the solution were taken every hour over 8 h (Figure 2b). A photodegradation chamber equipped with fluorescent, germicidal lamps emitting at a wavelength of 254 nm and with a power of 15 W was utilized. The samples were exposed to UV-C light, covering the range of 100 to 280 nm, and positioned 20 cm away from the lamps. Exposure durations lasted 12 min, with a maximum of 2 h, to ensure controlled exposure. This UV-C range was selected for its high energy, accelerating the aging of the samples. The photodegradation tests followed the methodology outlined by Cacuro *et al*.[15] The liquid obtained after desorption of the films (Figure 2c) was analyzed at each interval using UV-Vis spectroscopy.

Results and Discussion

Structural characterizations

The main bands found in the FTIR spectra of TPS (Figure 3a) and TPS-KL (Figure 3b) were as follows: O–H stretching bands in the region of 3100-3500 cm^{-1},[16] corresponding to the vibrations of hydroxyl bonds present in the starch structure, glycerol, and adsorbed water; C–H stretching bands between 2850-2950 cm^{-1}, attributed to the vibrations of C–H bonds from methyl and methylene groups in the glucose units and glycerol; a C=O stretching band in the range of 1650-1750 cm^{-1}, associated with carbonyl bonds, generally related to absorbed water or plasticizers; C–H bending vibrations between 1400-1460 cm^{-1}, originating from methyl and methylene groups; C–O stretching and C–O–H bending in the region of 1000-1200 cm^{-1}, characteristic of glycosidic bonds in starch and glycerol bonds; C–C and C–O–C stretching between 900-950 cm^{-1}, typical of glucose ring units in starch.[17]

From the spectra in Figure 3b, the addition of KL did not cause significant shifts in the bands, and the spectra were similar when compared to the TPS film spectrum in Figure 3a. These results may be due to the low concentration of lignin as a bio-additive, where the bands related to lignin overlapped the starch bands.[18] Changes were observed in the region of 3300 cm^{-1}, related to the characteristic vibrations of hydroxyl groups. A significant increase in the peak was observed at 2938 and 2869 cm^{-1}. According to Rodrigues and co-workers,[19] this region refers to the stretching vibrations normally attributed to the aliphatic C–H bonds of methyl and methylene groups. The spectrum of precipitated lignin shows bands at 1600, 1500, and 1400 cm^{-1}, which are attributed to vibrations of the aromatic skeleton and C–O absorption bands in phenolic hydroxyl groups at ca. 1200 cm^{-1}, confirming the nature of the compound.[8,20,21]

The analysis of the FTIR spectra provides insights into the differences in adsorption behavior between the TPS and TPS-KL films. The presence of kraft lignin introduces additional functional groups, such as aromatic rings and phenolic hydroxyls, which can interact with the dye molecules differently compared to the TPS matrix. The aromatic rings in lignin are capable of π-π interactions with the aromatic structures in dyes like MB and MO, potentially enhancing adsorption.[22] Additionally, the phenolic hydroxyl groups in lignin can form hydrogen bonds with dye molecules, further contributing to the adsorption process. These interactions are less pronounced in the pure TPS film, which relies more on hydroxyl groups from starch and glycerol for adsorption. Therefore, the difference in functional groups, as observed in the FTIR spectra, is a key factor in the enhanced adsorption capacity of the TPS-KL films compared to the pure TPS films.

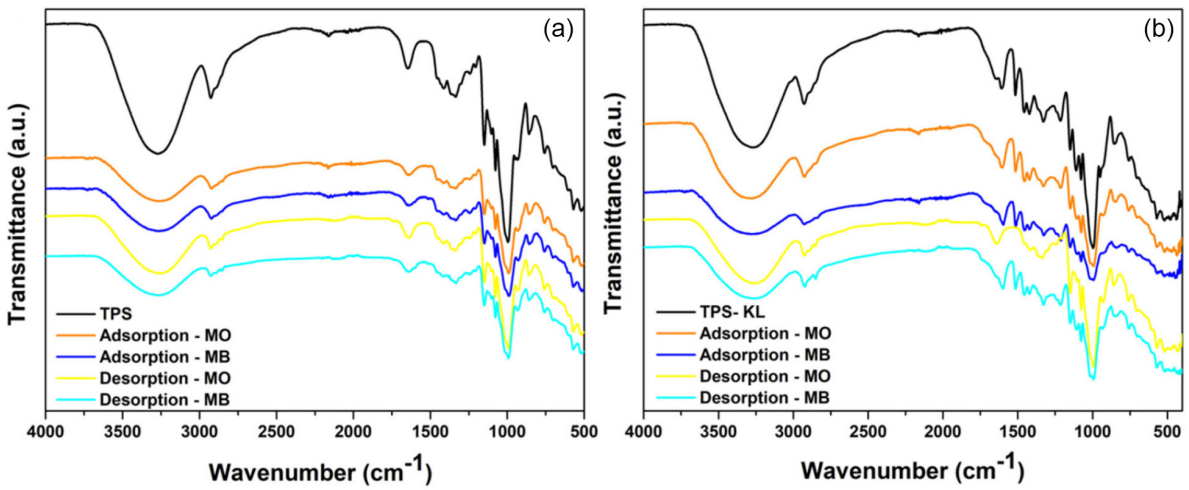

Figure 3. FTIR spectra: (a) TPS film and (b) TPS-KL film after adsorption/desorption in MB and MO solution at 10 mg L^{-1}.

The analysis of the FTIR spectra of TPS and TPS-KL films, after adsorption of MO and MB, and after desorption of MO and MB, showed that the spectra remained unchanged, without significant differences between them. This can be explained by the low dye concentration (10 mg L^{-1}), which may be insufficient to cause perceptible changes, and by the overlap of the characteristic bands of the dyes with the predominant bands of TPS. After desorption, the reversibility of the process and the absence of permanent chemical modification in the polymer matrix indicate that the adsorption/desorption process is physical, not chemical. The consistency in the spectra suggests that the adsorbent material can be reused without losing its basic structural properties.

Surface morphological changes

The SEM examination of both TPS and TPS-KL films provided valuable insights into surface morphology and the outcomes of dye adsorption and desorption processes. Chemically treated starches, when not gelatinized, maintained a granular structure, which could be observed microscopically as distinct starch granules[8] (Figure 4a). Both TPS and TPS-KL films displayed a rugged, uninterrupted surface marked with striations, a feature that enhances the contact area between the biosorbent and contaminants, thereby facilitating efficient adsorption.

After exposure to the solution and subsequent drying, the TPS-KL films became rigid and brittle. This change was evidenced in the micrographs, which show cracks after adsorption (Figure 4d) and desorption (Figure 4f), in contrast to the smoother surfaces of the TPS control films (Figures 4c and 4e). This brittleness can be attributed to the rigid nature of the lignin within the polymer matrix.

The micrographs revealed a lack of uniform dispersion of dye aggregates within the polymeric matrix, whether MB or MO, as observed in Figures 4 and 5. After dye

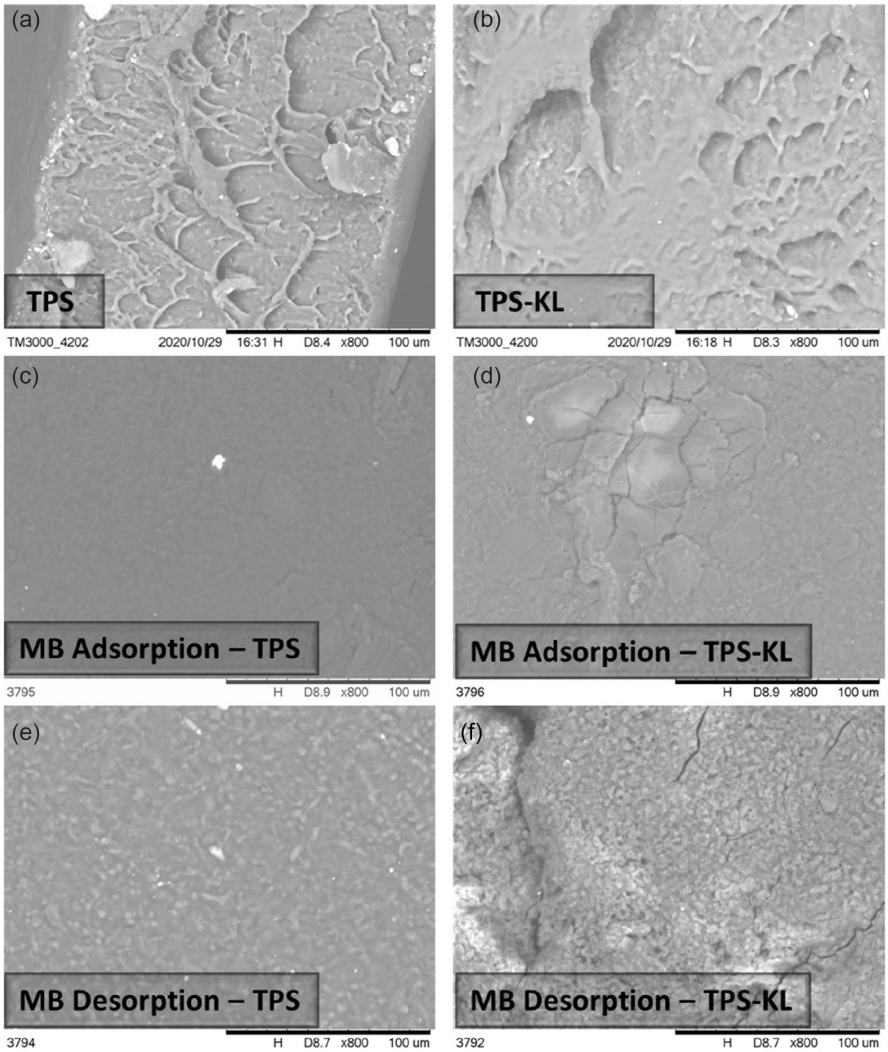

Figure 4. Micrographs of TPS (a), TPS-KL (b), TPS with adsorbed MB (c), TPS-KL with adsorbed MB (d), TPS with desorbed MB (e), and TPS-KL with desorbed MB samples (f).

adsorption, the surfaces of both TPS and TPS-KL films (Figures 4c and 4d; 5c and 5d) appeared smoother and more homogeneous compared to the original films (Figures 5a and 5b).

This smooth and homogeneous appearance can be attributed to the dye molecules filling in the irregularities and voids on the film surfaces, effectively coating rough areas and covering small surface features. As a result, the dye forms a continuous layer that masks the underlying texture, leading to a smoother surface after adsorption. This indicates successful dye adsorption, as the surface characteristics change, reflecting the coverage and interaction of the dye with the film.[23]

The SEM analysis showed that the addition of kraft lignin to TPS starch resulted in a rougher surface morphology compared to the pure TPS films.[24] This increased roughness is advantageous as it enhances the contact area between the biosorbent and contaminants, facilitating more effective adsorption. The development of a composite material with lignin and TPS starch not only altered the surface texture but also suggested improved adsorption properties. These findings indicate that lignin plays a significant role in enhancing the adsorption capabilities of TPS films by increasing their surface roughness, which is beneficial for contaminant removal processes.

Chemical characterizations

Ultraviolet-visible spectroscopy (UV-Vis)

The absorption spectra obtained in the visible region for the MO and MB dyes are shown in Figures 6a and 6b. The maximum absorption wavelengths are 465 nm for MO[25] and 600 nm for MB,[13] as previously reported.

Observing the results obtained in Figure 6b, it is possible to see that MB absorbs in the wavelength range

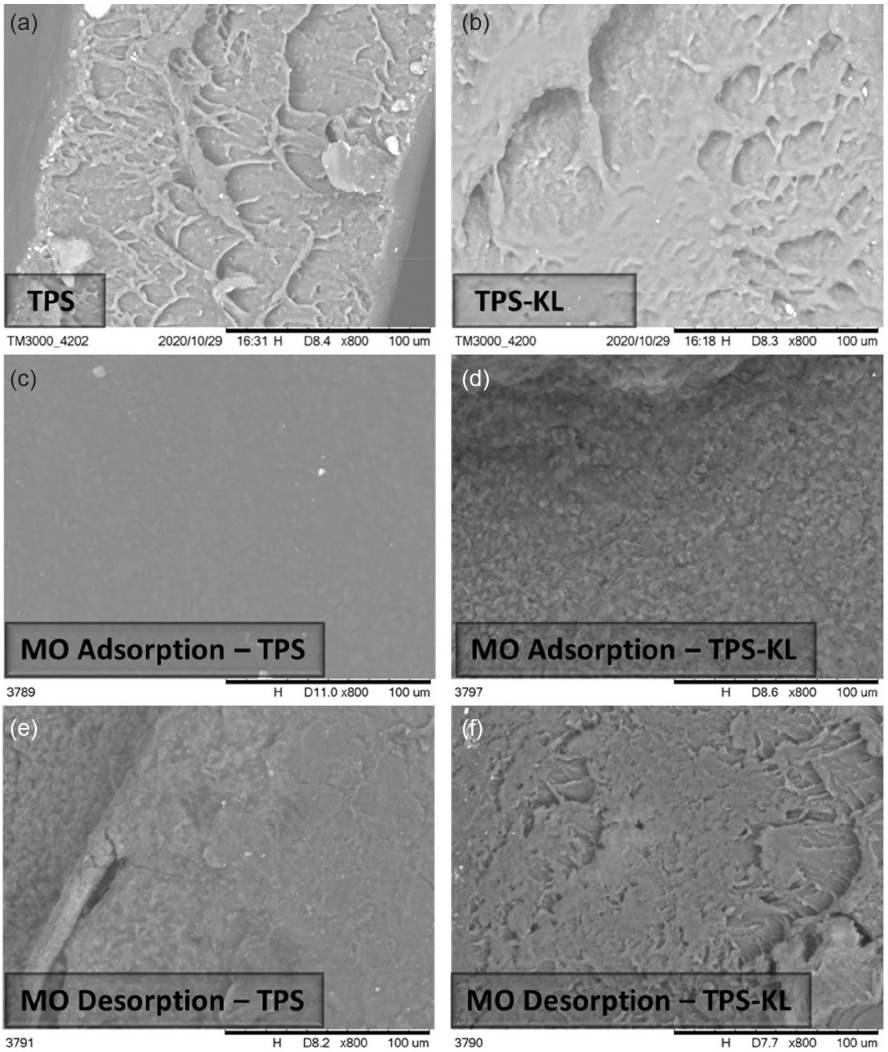

Figure 5. Micrographs of TPS (a), TPS-KL (b), TPS with adsorbed MO (c), TPS-KL with adsorbed MO (d), TPS with desorbed MO (e), and TPS-KL with desorbed MO samples (f).

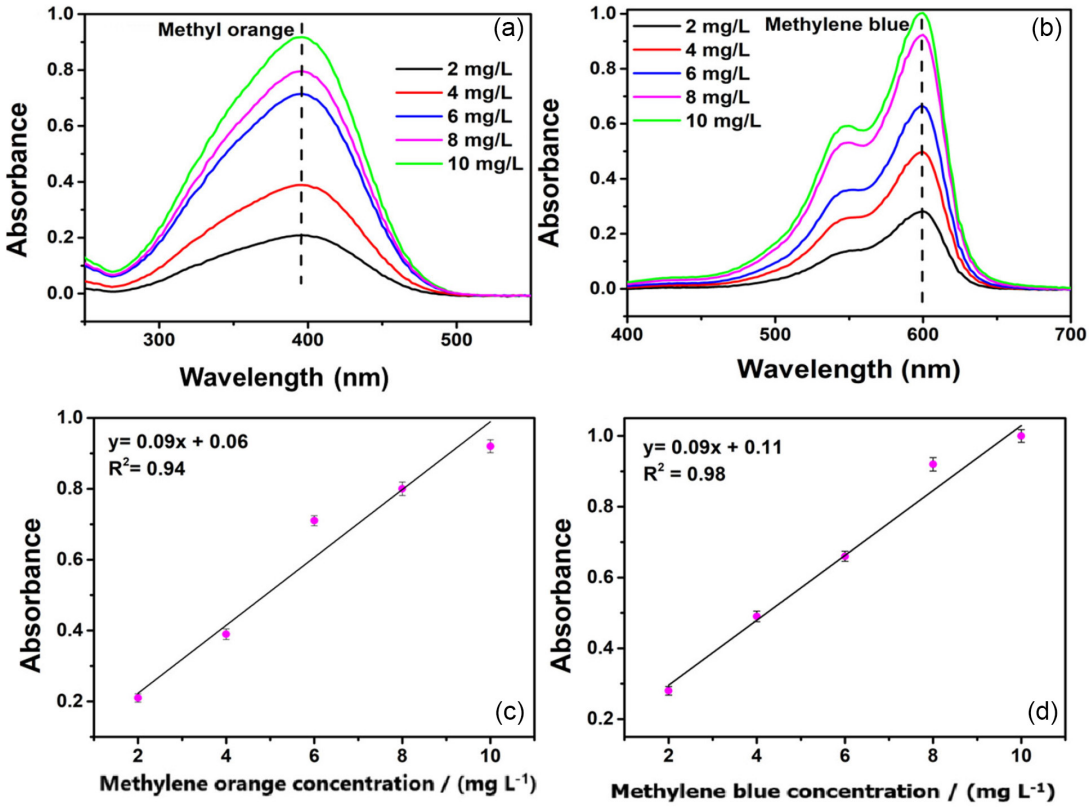

Figure 6. Absorption spectra in the UV-Vis region for the dyes: (a) MO and (b) MB in different concentrations. Analytical curves for dilutions of (c) MO in 465 nm and (d) MB in 600 nm.

of 600 nm and MO 465 nm (Figure 6a) and that in both cases the absorbance intensity meets the concentration of the dye solutions. It can be seen from the equations of the straight lines obtained that the values of the coefficients of correlation (R^2) were above 0.9 in the two analytical curves obtained (Figures 6c and 6d). This value can vary from 0 to 1 and the closer it is to 1, the more perfect the linearization of the points on the graph, indicating greater accuracy of the curves obtained and data from the samples that will be analyzed by UV-Vis.[26] The values of R^2 obtained were 0.94 and 0.98, that is, in both cases there is a correlation between the experimental data and the modeling theoretical (fitting) of around 94-98%, an acceptable correlation for the system studied.

Adsorption kinetics

Based on the results obtained by UV-Vis spectroscopy, it was possible to determine the concentration of the dyes adsorbed *per* hour. Figure 7a shows the results of the concentration of MO adsorbed by the TPS and TPS-KL samples. Both substrates showed low adsorption capacity of this dye with values close to 20% efficiency. The initial concentration in solution of 10 mg L^{-1} of MO dropped to approximately 8.5 mg L^{-1} for the TPS sample and to values close to 7.6 mg L^{-1} for the TPS-KL sample, which in turn showed a better result compared to pure TPS.

The improvement in MO adsorption capacity by TPS films with the addition of a percentage of KL has previously been reported in the literature.[8] Freitas *et al*.[8] also observed this effect, showing that TPS samples with 2 and 4% kraft lignin added had a higher capacity than TPS to remove the dye, however, they showed that at higher concentrations (8%) this effect is lost. This behavior was attributed mainly to the presence of functional groups, such as phenolic hydroxyl, hydroxyl alcohol, methoxyl, and carboxyl, in kraft lignin used as an additive. The study also did not observe a high rate of MO removal by the samples.

Based on this data, kinetic adjustments were made to the pseudo-first and pseudo-second-order models for each sample, and it was possible to obtain the R^2 and K values for each adjustment. The experimental data fit the pseudo-first or second-order model when the coefficients of determination are closer to 1. For the MO dye, the results obtained for the best-fitting kinetic model for each sample (TPS and TPS-KL) are shown in Figure 7b. For the TPS sample, a better fit was observed for the pseudo-second-order model with $R^2 = 0.998$ and $K = 0.349 \pm 0.01$, while for the TPS-KL sample, the adsorption kinetics obeyed the

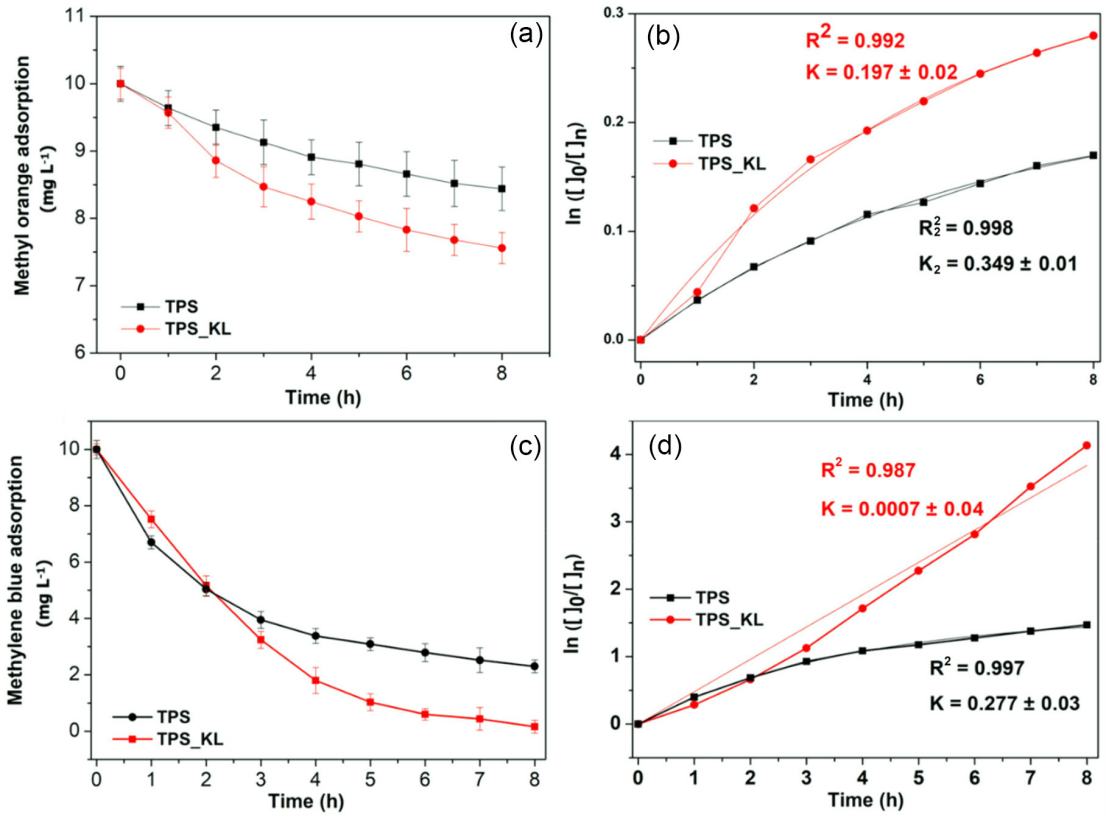

Figure 7. Results obtained by UV-Vis spectroscopy for the concentration of MO (a) and MB (c) adsorbed *per* hour of testing for the TPS and TPS-KL samples and their respective kinetic adjustments (b and d).

pseudo-first-order model with values of R^2 = 0.992 and K = 0.197 ± 0.02.

Figure 7c shows the results of the concentration of MB adsorbed by the TPS and TPS-KL samples. For MB, both samples showed an excellent adsorption rate of the dye, with values equal to or greater than 78% efficiency. The initial solution concentration of 10 mg L^{-1} of MB dropped to approximately 0 mg L^{-1} for the TPS-KL sample and to values close to 2.2 mg L^{-1} for the TPS sample. The better results observed for the adsorption efficiency of MB (ca. 80%) compared to MO (ca. 20%) can be explained by considering the chemical structures of the dyes and the films used. MO is an anionic dye, meaning it carries a negative charge.[3] MB, on the other hand, is a cationic dye with a positive charge.[4] The surface charge of the films and the interaction between these charges play a crucial role in adsorption. The films are primarily composed of starch, which is rich in hydroxyl groups that can form hydrogen bonds.[27]

Thus, the lower adsorption efficiency of MO may be due to weaker electrostatic interactions between the anionic dye and the starch-rich film surface, especially since the film has a similar charge and/or lacks sufficiently positively charged sites to attract the dye.[28] In contrast, MB, being cationic, can interact more strongly with negatively charged sites on the starch or polar groups on the film surface, resulting in greater adsorption.[29]

The superiority of the TPS-KL sample compared to TPS was also observed. This can be explained by the fact that starch has hydroxyl groups that can form weaker hydrogen bonds, while KL in the composition introduces aromatic rings and additional functional groups, such as methoxy and phenolic hydroxyl groups.[30] These structural differences can improve the interaction between the doped film and the dyes. This is particularly true for the TPS-KL film with MB, as the hydrophobicity of MB due to its aromatic structure can also result in stronger interactions with the hydrophobic regions in starch or lignin-containing films, increasing its adsorption[29] compared to methyl orange, which is more hydrophilic.

It was possible to observe through the curves that the adsorption capacity depends on the time of exposure to the dye. In general, adsorption capacity increased with increasing test time for all samples. It was also possible to conclude that the adsorption rate was initially fast (up to 4 h), and then slowed down (up to 7 h), reaching almost 100% adsorption (8 h) for the samples with lignin (TPS-KL) and equilibrium for the TPS sample in the last few hours.

Mohammadzadeh *et al.*[29] also studied the adsorption capacity of starch-based materials. Several factors,

including the relationship between time and adsorption efficiency, were analyzed in their study. The results obtained revealed a behavior like that reported in this study, in which the adsorption capacity increased over time, with adsorption being faster at the beginning until it stabilized and reached equilibrium after a period. This fact was attributed to the availability of active sites, which reflects rapid adsorption in the initial stages. The study also concluded that with an increase in MB concentration from 2 to 10 mg L^{-1}, the efficiency of the adsorbent increased. Rapo and Tonk[31] carried out a review of the literature on dye adsorption and desorption. Based on this review they concluded that in most studies the removal time ranged from 5 min to 36 h. However, maximum adsorption efficiency was reached in intervals of up to 5 to 60 min.

In this case, for MB dye (Figure 7d) the TPS-KL sample showed a better result than the TPS, although both were very efficient. For the TPS sample, the model with the best fit was the pseudo-first-order with values of $R^2 = 0.997$ and $K = 0.277 \pm 0.03$, unlike what happened for the same sample about the MO dye. For the TPS-KL sample, both dyes fitted the pseudo-first-order model, with $R^2 = 0.987$ and $K = 0.0007 \pm 0.04$ for MB.

Desorption of the dyes

Desorption studies help to explain adsorbate and adsorbent recovery, and the adsorption mechanism.[32] The samples that went through the dye adsorption process were used to study the desorption capacity of MO and MB in water. It is worth highlighting here that for MB there was almost total adsorption of the dye in solution by the samples, while for MO the adsorption capacity was around 20%. Therefore, it was expected that the amount of MB would be greater than that of MO for both samples (TPS and TPS-KL) as observed in Figure 8.

In Figure 8a we have data for the concentration of desorbed MO, considering the effect of time of contact in the desorption of the MO dye from the adsorbent coating. It was observed that the highest MO desorption efficiency occurred between the first and second tests, with the release of approximately 2 mg L^{-1} of the dye. After 2 h of desorption, there were no significant changes in the dye release capacity, which remained until the end of the test after 8 h. The desorbed concentration agrees with that adsorbed in the previous test, indicating the efficiency in desorption capacity was almost 100%. There were no considerable differences between the behavior of the TPS and TPS-KL samples, with the latter being slightly more efficient.

The desorption behavior as a function of MB dye contact time from the adsorbent coating was also evaluated, Figure 8b. It was observed that for the TPS sample, the highest MB desorption efficiency occurred between the first and second hours of testing with approximately 62% of the dye desorbed. Between 2 and 6 h desorption was slow, reaching a plateau (desorption close to 10%), however, between 6 and 8 h there was a further increase in the desorption speed reaching the maximum value of 10 mg L^{-1} of desorbed MB and returning, with the release of approximately 2 mg L^{-1} of dye. The desorbed concentration (10 mg L^{-1}) agrees with that adsorbed in the previous test, indicating the efficiency in desorption capacity.

The behavior of the TPS-KL sample was similar, being slightly more efficient in the desorption of MB as was seen for MO. However, the rapid desorption period extended up to 3 h of testing, with approximately 70% of the dye released. The interval between 3 and 7 h had a desorption rate moderate, with exponential behavior, which became rapid again in the last hour of the test, reaching almost total desorption of the MB.

The faster desorption of MO in relation to MB, can be explained by the same mechanism that led to the lower

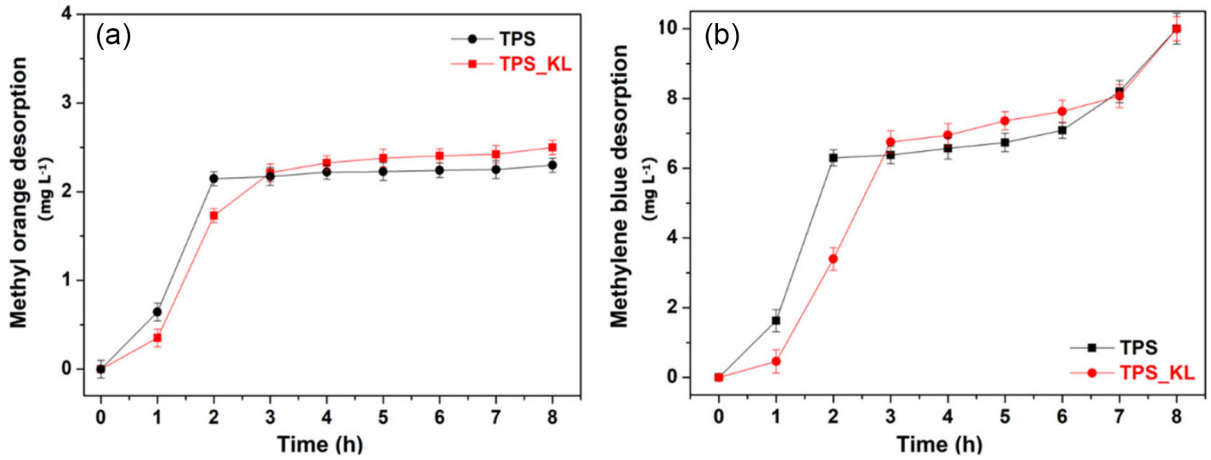

Figure 8. Results obtained by UV-Vis spectroscopy for the concentration of MO (a) and MB (b) desorbed *per* hour of testing for the TPS and TPS-KL samples.

adsorption of MO compared to MB. As mentioned earlier, the electrostatic interactions between MO and the film surfaces may be weaker, as the starch-based film surfaces might not have enough positive charges to efficiently retain MO, since it is not as strongly bound to the film as MB.[33] MO can form hydrogen bonds with the hydroxyl groups present in starch, but these bonds are relatively weak[28] compared to the possible interactions of MB with the polar and negatively charged groups on the film surface. As a result, MO can detach more easily from the film, leading to faster desorption. Additionally, MB, with its aromatic structure, tends to form stronger hydrophobic interactions with the film components, especially in the presence of KL, which also has hydrophobic characteristics.[34] These stronger interactions cause MB to be more retained in the film, resulting in slower desorption. Moreover, MO is more water-soluble than MB. This means that, once in contact with water, MO is more readily removed from the film surface, contributing to faster desorption.

Dyes remediation by photodegradation

Among the various strategies adopted for the remediation of dyes from water bodies, adsorption itself, coagulation-flocculation, bioremediation and photodegradation stand out.[35] The latter was chosen in this study because it does not require the addition of more chemicals, as it uses light (generally UV) and generates reactive oxygen species capable of decomposing the dyes into less toxic and more biodegradable products. Photodegradation can be highly efficient in removing a wide range of dyes, including those that are resistant to other treatment methods.[36]

After desorption of the dyes in water, photodegradation of these solutions was carried out, the process was monitored by UV-Vis measurements of the solution at different time intervals, Figure 9. This procedure was carried out to eliminate MB and MO, since environmental remediation of dyes in water is a significant challenge due to the persistence and toxicity of these compounds.

The MO solution desorbed from the TPS had its photodegradation process monitored, and the results are presented in Figure 9a. The graph shows the results of the linear regression carried out based on the maximum absorbance value at 465 nm, the characteristic region of MO. It is possible to observe a decreasing behavior of absorbance as a function of increasing the light exposure interval, with a value of $R^2 = 0.82$. The same process was carried out for MB desorbed from TPS, Figure 9b, using the maximum absorbance of the band centered at 600 nm. For this sample, the process of luminous degradation of the dye was also decreasing, indicating a reduction in the presence of the dye in the water, with a good capacity for

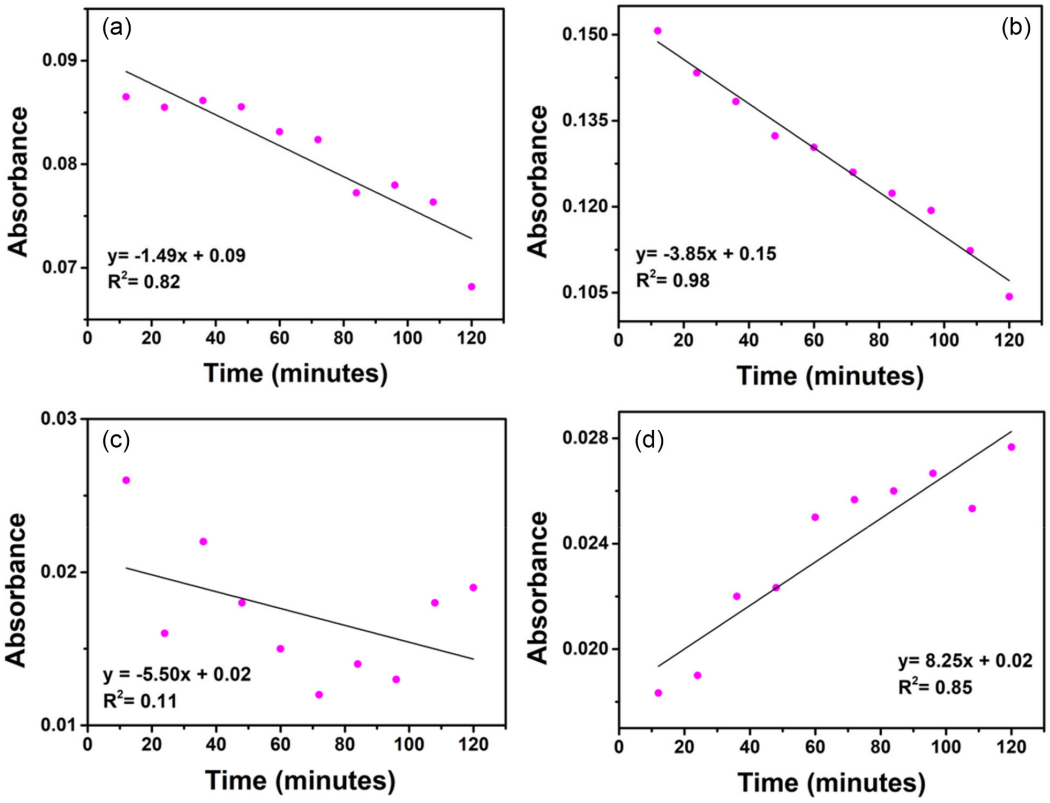

Figure 9. Linear regressions plots of samples photodegradation rate: (a) TPS/MO, (b) TPS/MB, (c) TPS/MB and (d) TPS-KL/MB samples.

progressive elimination, with $R^2 = 0.98$, showing a better result in the remediation of MB about MO.

This superiority in the remediation of MB compared to MO can be explained by the action of light on the chemical structure of the dyes. MB is known to be more susceptible to photodegradation under light, especially visible and UV light. Its chemical structure contains a conjugated system of aromatic rings and double bonds that can be more easily broken by the energy provided by light, inducing the formation of reactive oxygen species that attack the structure of the dye, resulting in its faster degradation. MO, on the other hand, may be more resistant to this process due to its chemical structure, which may not absorb light in the same way or generate the same reactive oxygen species.[37] MB has an absorption spectrum that better overlaps with visible light, making it more susceptible to photodegradation when exposed to sunlight or UV light.[38] MO may have an absorption spectrum that does not correspond well to the light used, resulting in lower degradation efficiency. In summary, the better elimination of MB compared to MO in the presence of light can be attributed to the greater sensitivity of MB to photodegradation, facilitated by its chemical structure and absorption spectrum, which allows for greater interaction with light.

For the MO solution desorbed from TPS-KL, the photodegradation test was not effective, as there was no significant pattern in the variation of intensity by the accompanying band (465 nm) during the test interval, with $R^2 = 0.11$, Figure 9c. This can be attributed to the low concentration of dye in the solution and the presence of KL in the solution, which has photoprotective properties. As studied by Rodrigues *et al*.,[20] the addition of KL and its fractions in TPS films provided less photodegradation of these composites, being attributed to the OH groups of the guaiacyl phenolic units, abundant in KL, which increased the ultraviolet absorption capacity, guaranteeing a greater photoprotective effect to the film.

For the MB solution desorbed from TPS-KL, it was possible to monitor the photodegradation process, and the results are presented in Figure 9d. The graph shows the results of the linear regression carried out based on the maximum absorbance value at 600 nm, where it is possible to observe an increasing behavior of absorbance as a function of the increase in the light exposure interval, with a value of $R^2 = 0.85$. The growth in intensity is analogous to the expected behavior. It can be attributed to the photoprotection of the dye carried out by KL as previously mentioned and/or the formation of new reactive species in the same monitoring region, requiring further study. Therefore, it can be concluded that remediation by direct photodegradation needs to be better investigated in this application, with the photocatalytic degradation of these dyes, using a catalyst, also being a possible strategy.[36,39]

Conclusions

This study explored the use of thermoplastic starch (TPS) and kraft lignin (KL) composites for water treatment, focusing on their ability to remove dyes such as methylene blue (MB) and methyl orange (MO) through adsorption/desorption and photodegradation. TPS and TPS-KL films were considered as good possible adsorbents due to their properties and porous surfaces. The incorporation of KL into TPS led to an increase in surface roughness, which enhanced the contact area available for dye adsorption. This improvement may explain the superior performance observed with the TPS-KL composite compared to TPS alone. FTIR analysis confirmed that the dyes were physically adsorbed, which facilitates the reuse of the adsorbents. UV-Vis spectroscopy further supported these results, demonstrating a significantly higher removal efficiency for MB (close to 100%) compared to MO (25%). Additionally, pseudo-first-order kinetic models were proposed for the adsorption of MB and MO on TPS-KL and MB/TPS, while pseudo-second-order models were applied to TPS/MO. Regarding desorption, the TPS-KL samples were more efficient for both dyes. The photodegradation of the desorbed dyes showed promising results for the two dyes desorbed from the TPS substrate. However, for the TPS-KL substrate, the results obtained require further investigation to become conclusive.

Acknowledgments

This work was funded by Fundação de Amparo à Pesquisa do Estado de São Paulo (FAPESP, 2023/06505 (M. F.), 2023/17363-0 (A. S. M. F.), 2023/00335-4 (J. S. R.) and 2014/50869-6 (INE0)); Conselho Nacional de Desenvolvimento Científico e Tecnológico (CNPq, 169054/2023-3 (S. F. A.)) and project 14805 - Finep 01.22.0179.00 (MARTMA).

References

1. Pereira, R. S.; *Rev. Eletrônica Recur. Hídricos* **2004**, *1*, 20. [Link] accessed in September 2024
2. Dutta, S.; Adhikary, S.; Bhattacharya, S.; Roy, D.; Chatterjee, S.; Chakraborty, A.; Banerjee, D.; Ganguly, A.; Nanda, S.; Rajak, P.; *J. Environ. Manage.* **2024**, *353*, 120103. [Crossref]
3. Abewaa, M.; Adino, E.; Mengistu, A.; *Heliyon* **2023**, *9*, e22447. [Link] accessed in September 2024

4. Munonde, T. S.; Nqombolo, A.; Hobongwana, S.; Mpupa, A.; Nomngongo, P. N.; *Heliyon* **2023**, *9*, e15502. [Crossref]
5. do Nascimento, R. F.; de Lima, A. C. A.; Vidal, C. B.; Melo, D. Q.; Raulino, G. S. C.; *Adsorção: Aspectos Teóricos e Aplicações Ambientais*, 2nd ed.; Imprensa Universitária: Fortaleza, 2014.
6. De Bortoli, Á. L.; Andreis, G. S. L.; Pereira, F. N. In *Modeling and Simulation of Reactive Flows*; De Bortoli, Á. L.; Andreis, G. S. L.; Pereira, F. N., eds.; Elsevier: Amsterdam, Oxford, Waltham, 2015, ch. 1, p. 1-10. [Crossref]
7. Qin, Y.; Liu, C.; Jiang, S.; Xiong, L.; Sun, Q.; *Ind. Crops Prod.* **2016**, *87*, 182. [Crossref]
8. de Freitas, A. S. M.; Rodrigues, J. S.; Maciel, C. C.; Pires, A. A. F.; Lemes, A. P.; Ferreira, M.; Botaro, V. R.; *Int. J. Biol. Macromol.* **2021**, *184*, 863. [Crossref]
9. Yang, L.; Paulson, A. T.; *Food Res. Int.* **2000**, *33*, 563. [Crossref]
10. *Origin Pro*, version 8.5; OriginLab Corporation, Northampton, Massachusetts, USA, 2008.
11. *Microsoft Power Point software*, version Microsoft 365; Microsoft Corporation, Redmond, Washington, USA, 2011.
12. Silva, L. P. A.: *Síntese e Caracterização de Novos Polímeros Conjugados Derivados de Tiofeno-Pirrol-Tiofeno (SNS) Ligados aos Corantes Azo Alaranjado de Metila e Vermelho de Metila*; MSc Dissertation, Universidade Federal de Alagoas, Alagoas, Brazil, 2020. [Link] accessed in September 2024
13. Quirk, B. J.; Brandal, G.; Donlon, S.; Vera, J. C.; Mang, T. S.; Foy, A. B.; Lew, S. M.; Girotti, A. W.; Jogal, S.; LaViolette, P. S.; Connelly, J. M.; Whelan, H. T.; *Photodiagn. Photodyn. Ther.* **2015**, *12*, 530. [Crossref]
14. Moura, A. L. A.; de Oliveira, L. K.; Ciuffi, K. J.; Molina, E. F.; *J. Mater. Chem. A* **2015**, *3*, 16020. [Crossref]
15. Cacuro, T. A.; Freitas, A. S. M.; Waldman, W. R.; *J. Chem. Educ.* **2018**, *95*, 2222. [Crossref]
16. Wei, Z.; Cai, C.; Huang, Y.; Wang, P.; Song, J.; Deng, L.; Fu, Y.; *Int. J. Biol. Macromol.* **2020**, *164*, 27. [Crossref]
17. Ferreira, L. F.; de Oliveira, A. C. S.; Begali, D. O.; Sena Neto, A. R.; Martins, M. A.; de Oliveira, J. E.; Borges, S. V.; Yoshida, M. I.; Tonoli, G. H. D.; Dias, M. V.; *Ind. Crops Prod.* **2021**, *160*, 113092. [Crossref]
18. Araújo, L. C. P.; Yamaji, F. M.; Lima, V. H.; Botaro, V. R.; *Bioresour. Technol.* **2020**, *314*, 123757. [Crossref]
19. Amaro, S. F.; Maciel, C. C.; Rodrigues, J. S.; de Freitas, A. S. M.; Fré, L. V. B. V.; de Barros, A.; Ferreira, M.; *Chemosensors* **2023**, *11*, 420. [Crossref]
20. Rodrigues, J. S.; de Freitas, A. S. M.; Lopes, H. S. M.; Pires, A. A. F.; Lemes, A. P.; Ferreira, M.; Botaro, V. R.; *Int. J. Biol. Macromol.* **2023**, *230*, 123142. [Crossref]
21. Rodrigues, J. S.; Senna, A. M.; de Oliveira, C. T.; Botaro, V. R.; *Ind. Crops Prod.* **2021**, *166*, 113492. [Crossref]
22. Fattahi, M. T.; Dadashian, F.; Mir, M. S. G.; Ebrahimi, Z. A. H.; *Powder Technol.* **2014**, *261*, 232. [Crossref]
23. Oladipo, M. A.; Bello, I. A.; Adeoye, D. O.; Abdulsalam, K. A.; Giwa, A. A.; *Adv. Environ. Biol.* **2013**, *7*, 3311. [Link] accessed in September 2024
24. Kargarzadeh, H.; Galeski, A.; Pawlak, A.; *Polymer* **2020**, *203*, 122748. [Crossref]
25. Zhang, A.; Fang, Y.; *Chem. Phys.* **2006**, *331*, 55. [Crossref]
26. Chein, F.; *Introdução aos Modelos de Regressão Linear: Um Passo Inicial para Compreensão da Econometria como uma Ferramenta de Avaliação de Políticas Públicas*; Enap: Brasília, 2019. [Link] accessed in September 2024
27. Freitas, A. S. M.; Silva, A. P. B.; Montagna, L. S.; Nogueira, I. A.; Carvalho, N. K.; de Faria, V. S.; dos Santos, N. B.; Lemes, A. P.; *J. Biomater. Sci., Polym. Ed.* **2022**, *33*, 900. [Crossref]
28. Mallakpour, S.; Rashidimoghadam, S.; *Carbohydr. Polym.* **2017**, *169*, 23. [Crossref]
29. Mohammadzadeh, F.; Golshan, M.; Haddadi-Asl, V.; Salami-Kalajahi, M.; *Sci. Rep.* **2023**, *13*, 11900. [Crossref]
30. Park, S. Y.; Kim, J. Y.; Youn, H. J.; Choi, J. W.; *Int. J. Biol. Macromol.* **2018**, *106*, 793. [Crossref]
31. Rapo, E.; Tonk, S.; *Molecules* **2021**, *26*, 5419. [Crossref]
32. Şentürk, İ.; Alzein, M.; *Acta Chim. Slov.* **2020**, *67*, 55. [Crossref]
33. Pliego-Arreaga, R.; Regalado, C.; Amaro-Reyes, A.; García-Almendárez, B. E.; *Rev. Mex. Ing. Quim.* **2013**, *12*, 505. [Link] accessed in September 2024
34. Fernández-Rodríguez, J.; Erdocia, X.; Hernández-Ramos, F.; Alriols, M. G.; Labid, J. In *Separation of Functional Molecules in Food by Membrane Technology*; Galanakis, C. M., ed.; Academic Press: Amsterdam, 2019, p. 265. [Crossref]
35. Tripathi, M.; Singh, S.; Pathak, S.; Kasaudhan, J.; Mishra, A.; Bala, S.; Garg, D.; Singh, R.; Singh, P.; Singh, P. K.; Shukla, A. K.; Pathak, N.; *Toxics* **2023**, *11*, 940. [Crossref]
36. Rafiq, A.; Ikram, M.; Ali, S.; Niaz, F.; Khan, M.; Khan, Q.; Maqbool, M.; *J. Ind. Eng. Chem.* **2021**, *97*, 111. [Crossref]
37. de Sá, F. P.; Nunes, L. M.; *Rev. Processos Quim.* **2017**, *11*, 77. [Crossref]
38. Pereira, R. A.; Brito, N. N.; *Holos Environ.* **2013**, *13*, 74. [Link] accessed in September 2024
39. Khan, I.; Saeed, K.; Ali, N.; Khan, I.; Zhang, B.; Sadiq, M.; *J. Environ. Chem. Eng.* **2020**, *8*, 104364. [Crossref]

Submitted: June 26, 2024
Published online: October 11, 2024